CHAPTER 4

A comprehensive evaluation of the integrated photocatalytic-fixed bed bioreactor system for the treatment of Acid Blue 113 dye

CHAPTER 4

A comprehensive evaluation of the integrated photocatalytic-fixed bed bioreactor system for the treatment of Acid Blue 113 dye

4.1 Introduction

Previously, a wide range of physicochemical and biological methods have been developed for the treatment of complex dyes (Swain et al., 2021). However, biological methods are not always effective in completely degrading complex dyes compounds in a reasonable time due to their biological and chemical stability (Dargahi et al., 2021). A promising alternative is the pre-treatment to enhance the biodegradability of such kinds of organic compounds (Malik et al., 2019). In the last few decades, research has inclined to investigate more efficient techniques that can degrade the compounds with less sludge generation (Jorfi et al., 2018). AOPs are increasingly being explored as a highly efficient process for assorted wastewaters, notably toxic and biorecalcitrant textile effluents (Mohammadzadeh et al., 2015). Interestingly, textile wastewater treatment employing AOPs leading up to biological treatment enables the creation of simple and most economical wastewater treatments (Doumic et al., 2015). The most widespread AOPs are Photocatalysis, Photo-Fenton, Ozonation, Electrochemical oxidation, and Sonolysis (Kanakaraju et al., 2018). Among AOPs, Photocatalysis has attracted significant interest in the degradation of recalcitrant constituents in aqueous solutions (Takdastan et al., 2018). Thus, the integration of Photocatalysis and Biodegradation technologies could be a vital approach to the complete degradation of complex dye wastewater.

Based on the author's knowledge, very limited efforts have been given to develop the integrated system (Photocatalysis + Biodegradation) for the treatment of complex dye Acid Blue 113 (AB 113) from wastewater. The present study aims to investigate the performance of a hybrid

system, i.e., a Photocatalytic reactor followed by a Fixed-bed bioreactor. AB113 was selected as the model contaminant due to its chemical stability and resilience to low biodegradability. The photocatalytic pre-treatment efficiency, as well as the biodegradability of the treated solutions, were investigated. Furthermore, the effects of dye concentration, pH, and TiO_2 loading were examined. The bioreactor's effectiveness against dye shock loading was also assessed. The bacterial toxicity analysis of degraded products was also performed to validate the efficacy of the integrated process.

4.2 Materials and methods

4.2.1 Dye and chemicals

Acid Blue 113 [$C_{32}H_{21}N_5Na_2O_6S_2$, Molecular Weight: 681.65, CAS number: 3351-05-1], a di-azo dye, was purchased from Sigma-Aldrich, India. Anatase Titanium (IV) Oxide, (TiO_2) powder (Purity 99.9%, Molecular Weight: 79.87) was used as a photocatalyst. MSM used in the present study has the same composition as mentioned in section 3.2.1. The composition and chemical properties of AB 113 wastewater are listed in **Table 4.1**.

Table 4.1 Acid Blue 113 Wastewater Characteristics.

S.N.	Acid Blue 113 wastewater Characteristics	Concentrations
1.	AB 113 Concentration	300 mg/L
2.	pH	7.5 ± 0.5
3.	Chemical Oxygen Demand (COD)	1256 ± 22.8 mg/L
4.	Biochemical oxygen demand (BOD)	264 ± 4.6 mg/L
5.	Total Organic Carbon (TOC)	678.8 ± 13.9 mg/L
6.	Electrical Conductivity	2.59 mS/cm

4.2.2 Microorganism

The potential bacterial species were isolated from the textile effluents contaminated soil of nearby textile industrial regions of Varanasi, India, as discussed in section 3.2.2. A potential bacterial species, i.e., *Klebsiella michiganensis* strain DP2ZMA43 (Accession No. MH972172) was used for biodegradation of AB 113. The phylogenetic tree of bacterial species is illustrated in **Figure 4.1**.

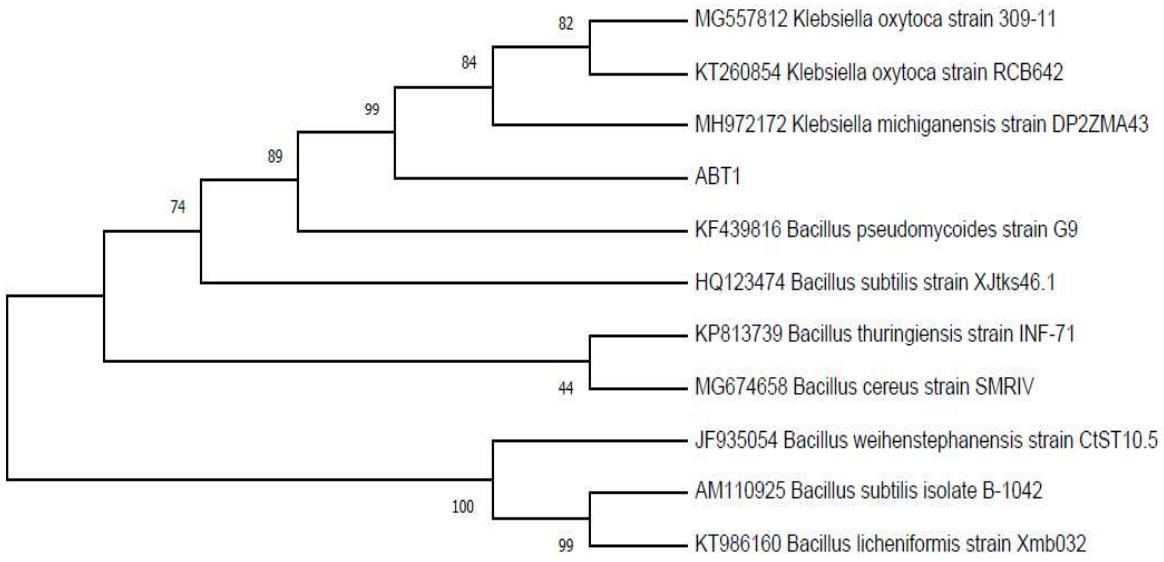

Figure 4.1. Phylogenetic tree of isolated bacterial species *Klebsiella michiganensis*

4.2.3 Hybrid Photo-Bioreactor configuration

The experimental hybrid reactor set-up consists of a 200 mL Photocatalytic reactor (PC) followed by a Fixed-bed Bioreactor (FBR) (600 mL of capacity). Both of the reactors were operated in semi-batch mode, as illustrated in **Figure 4.2**. The microbial growth can be inhibited through the moderate irradiation of UV light by damaging their DNA. UV light disrupts the genetic material, preventing normal cellular functions and reproduction. This is often used as a method for disinfection in water treatment and sterilization processes. However, in a sequential Photocatalytic Oxidation-Fixed Bed Bioreactor system, the microorganisms

were not exposed to direct UV irradiation. The UV light was irradiated into the Acid Blue 113 solution without inoculum of bacterial species. Additionally, the UV irradiation attenuates as the dye solution concentration increases.

4.2.3.1 Photocatalytic experiments

The photocatalytic reactor was comprised of a plexiglass cylinder having an inner diameter and height of 4 cm and 60 cm, respectively. The reactor was illuminated by two cylindrical UV lamps (125 W, 368 nm, light intensity 2.0×10^{-3} E s^{-1}) with consistent dispersion and the reaction medium was magnetically stirred at 250 rpm. The outer surface of the cylinder was covered with reflective aluminum foil to prevent interference with visible light from the surroundings. During each experimental run, the reaction temperature in the photocatalytic reactor was maintained through the use of a controlled heating system by thermostat. This ensures a constant temperature conducive to photocatalytic oxidation and allows efficient heat dissipation and stabilization.

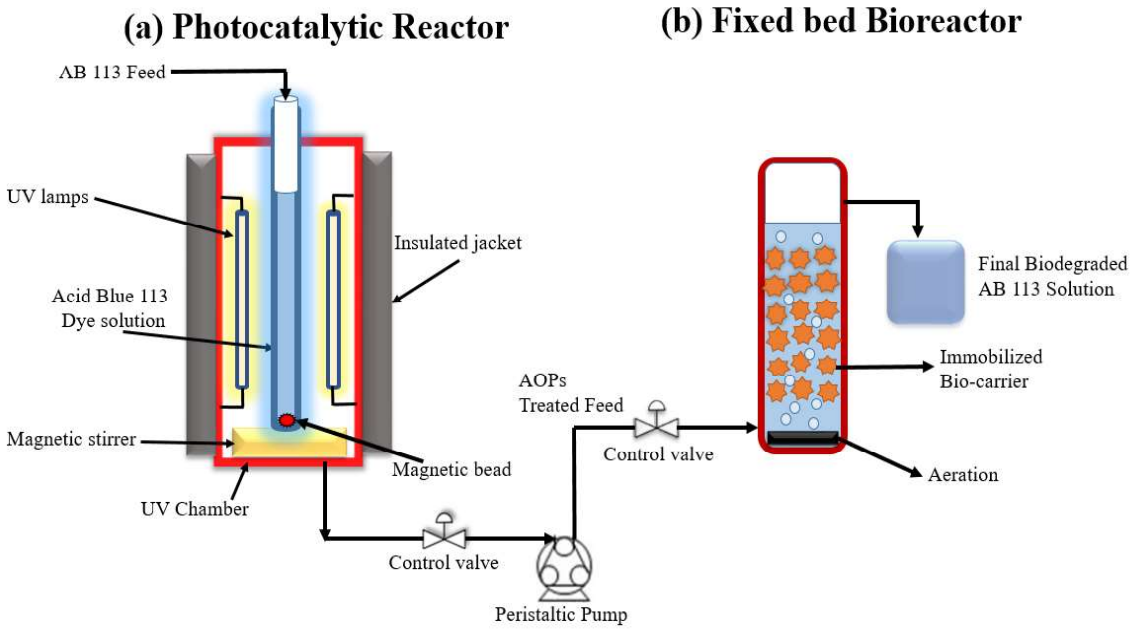

Figure 4.2. Experimental Hybrid reactor setup: (a) Photocatalytic reactor; (b) Fixed bed Bioreactor

4.2.3.2 Biological experiments: Fixed-bed Bioreactor (FBR)

An FBR (ID 5.6 cm, length 65 cm) was made up of borosilicate glass. The inlet and outlet ports were provided at a distance of 10 cm from the bottom and top of FBR for sampling. The pH and dissolved oxygen levels of 7.0 ± 0.5 and 7 ± 1.5 mg/L, respectively were maintained in a bioreactor. Polyurethane foam (PUF) (2×2 cm, cubes) were selected as the support packing material for the *Klebsiella michiganensis* immobilization. The effluent received after photocatalytic oxidation was supplied into FBR for further mineralization. The media (Nutrient broth + mineral salt media) proliferate the biofilm formation on the surface of PUF and the reactor was operated under aerobic conditions. The volumetric flow rate of oxygen was maintained at 2 L/min using a rotameter (Flow point, India). The dye solution was fed with varying flow rates to the reactor entrance using a Peristaltic pump (ELECTROLAB, PP- 50V). The entire biodegradation study was performed under an ambient (Temperature = 35 ± 3 °C).

4.2.4 Characterization of Photocatalyst and degraded compounds

Anatase TiO_2 particle size distribution and zeta potential were measured by Zeta Potential analyzer (Malvern Panalytical, Zetasizer Ver. 7.13, Serial Number: MAL1213575). Distilled water has a refractive index (RI) of 1.330 and a dielectric constant of 78.5, which was used as a dispersant for completely dispersing TiO_2 particles (RI = 2.70). The extent of dye mineralization was assessed in terms of reduction in COD and TOC. The COD, BOD and TOC of the sample was determined, as mentioned in section 3.2.4. Ethyl acetate (v/v) was used to extract the degraded intermediate compounds from both processes from the solution and anhydrous Na_2SO_4 was used to dehydrate them. These extracted compounds were allowed to further concentrate using a rotary vacuum evaporator and finally mixed with HPLC grade methanol. FTIR (Nicolet iS5, THERMO) was used to elucidate the functional group of photocatalytically oxidized as well as biodegraded samples.

4.2.5 Photocatalytic and Biodegradation Kinetic study

4.2.5.1 Development of a mathematical model for photocatalytic oxidation

Langmuir-Hinshelwood mathematical equation, adapted for reactions that take place over the liquid-solid interface, is used to evaluate the influence of initial dye concentration on the removal of dye over TiO_2 surfaces (Sharma et al., 2012). It is commonly employed in the study of surface reaction kinetics. During photocatalysis, the rate of reaction can then be stated as:

$$-R_p = \frac{dC}{dt} = \frac{k_c\ K_c\ C}{1+K_c\ C+\Sigma\ K_I\ C_i} \tag{4.1}$$

where R_p is the rate of reaction, C and C_i represent the inlet and outlet concentration of dye, respectively, t is the processing time for photocatalytic oxidation, and k_c is the Langmuir reaction rate constant. K_C and K_I are the adsorption equilibrium constants for dye and intermediate compound I, respectively. Since dye decolorization kinetics in bulk solution follows pseudo-first-order kinetics concerning concentration:

$$-R_p = \frac{dC}{dt} = ln\ (\frac{C}{C_o}) = -\ k_{approx}\ C \tag{4.2}$$

Additionally, the following assumption can be made only when it is predicted that the adsorption equilibrium constants of every organic molecule existing in the reaction solution are also almost equal:

$$\Sigma\ K_I\ C_I + K_c\ C = K_c\ C_o \tag{4.3}$$

where C_o is the initial dye concentration. The combined adsorption equilibrium constant of the dye and its derivatives is designated by K_c in the equation above. Combining the equations (4.1), (4.2), and (4.3) the following relation is obtained:

$$\frac{1}{k_{approx}} = \frac{1}{k_c\ K_c} + \frac{C_0}{k_c} \tag{4.4}$$

the equation (4.4) is used for the analysis of k_c and K_C by making a plot between $\frac{1}{k_{approx}}$ vs C_o.

4.2.5.2 Growth kinetics study and inhibition of Acid Blue 113 during biodegradation

For the fixed bed bioreactor system, the biodegradation process is dominated by the biochemical reaction, and therefore adsorption and diffusion effects can be neglected (Sen et al., 2017). In this study, the Monod model (Eq. 4.5) has been used to predict the response in the biodegradation process under non-inhibitory conditions (Geed et al., 2017). This model illustrates how microbial growth is influenced by the availability of nutrients in their environment. It suggests that microbial growth has two main phases: a rapid growth phase when the substrate (nutrient) is abundant, and a slower growth phase as the substrate becomes limited.

$$\mu = \frac{1}{X}\frac{dX}{dt} = \frac{\mu_{max} S}{K_S + S} \tag{4.5}$$

where μ = specific growth rate (day^{-1}); μ_{max} = maximum specific growth rate (day^{-1}); K_s = half-saturation constant (mg/L) indicating the substrate concentration at which growth rate is half of the maximum; X = bacterial cell concentration (mg/L); S = initial substrate concentration (mg/L); t = Bioreactions process time (days)

After rearranging in linearized form the Monod model becomes:

$$\frac{1}{\mu} = \frac{K_S}{\mu_{max} S} + \frac{1}{\mu_{max}} \tag{4.6}$$

Eq. (4.6) was allowed to fit the experimental data to obtain the values of maximum specific growth rate (μ_{max}) and half-saturation constant (K_s).

Under a higher substrate loading rate, the Monod equation fails to provide satisfactory due to substrate inhibition (Sonwani et al., 2020). Therefore, the Andrews Haldane model was employed to evaluate the substrate inhibition constant K_i (mg/L) under a high loading rate. Andrew Haldane equation is given below for the assessment of inhibition kinetics (Sonwani et al., 2021b):

$$\mu = \frac{\mu_{max}\ S}{K_S + S + \frac{S^2}{K_i}} \quad (4.7)$$

where μ_{max} is the maximum specific growth rate (day^{-1}), K_i is the substrate inhibition constant (mg/L), S is the substrate (AB 113) concentration (mg/L) and K_s is the half-saturation constant (mg/L). The Andrews-Haldane equation unveils the complexities of substrate inhibition kinetics, offering insights into how substrate concentration influences enzyme activity, particularly in the presence of inhibitory effects.

4.2.6 Bacterial toxicity assessment

Bacterial toxicity assessment is an innovative technique used to understand the potential harmful effects of substances on bacterial organisms. This approach involves subjecting bacteria to different concentrations of a substance to observe changes in their growth. The toxicity analysis is the most widely used technique to evaluate the adverse impacts of intermediate products produced during the hybrid treatment process. The bacterial species *Vibrio Harvey*, *Vibrio fischeri, P. luminescens subsp akhurstii,* and *Pseudomonas fluorescens* are bioluminescent and widely employed for toxicity analysis (Chaturvedi et al., 2021; Gatidou et al., 2015). Before analysis, the samples were centrifuged at 5000 rpm for 20 min, filtered with 0.44 µm filter paper, and finally sterilized. In this work, *Pseudomonas fluorescens*, a bioluminescent bacterial species was used for analyzing the chronic and acute toxicity levels. Sterilized distilled water was used as a control. The bacterial culture having an optical density (OD 600 nm) of about 1 was used with treated samples. 1 mL bacterial culture was simultaneously added to 10 mL each of control, AB 113, photocatalytic oxidized, and biodegraded samples. The bioluminescence intensity in terms of counts per second of each sample was measured with a Horiba Fluorescence spectrophotometer (PTI QuantaMaster™ 8000 series). After the addition of *Pseudomonas fluorescens,* samples were collected at an incubation duration of 30 min and 24 hr for the assessment of acute and chronic toxicities,

respectively. Bioluminescence inhibition assays provide rapid and sensitive insights into the potential harmful effects of chemicals, pollutants, or environmental factors on living systems. The degree of inhibition in their light emission serves as an indicator of the substance's toxic effects. The bioluminescence inhibition percentage for each treated sample was calculated with respect to the control sample using the following formula:

$$\text{Bioluminescence Inhibition \%} = \frac{\text{Control Intensity} - \text{Sample Intensity}}{\text{Control Intensity}} \times 100 \quad (4.8)$$

4.3 Results and Discussion

4.3.1 Photocatalyst (TiO_2) Characterization

Anatase TiO_2 having a band gap of 3.2 eV was used as a photocatalyst during the pretreatment of AB 113. The average particle size of TiO_2 was 501.6 nm (**Figure 4.3a**). The Polydispersity index (PdI) of 0.211 was reasonable in the fact that the photocatalyst had a uniform and large size distribution in the aqueous solution. The net surface charge i.e., the zeta potential of -25.1 mV indicated that the colloidal solution formed after the complete dispersion of TiO_2 was relatively stable (**Figure 4.3b**). The electrical conductivity and zeta deviations were 0.0103 mS/cm and 5.61 mV, respectively. The above key finding indicated that the TiO_2 particles were dispersed uniformly throughout the dye solution and formed a stable colloidal solution.

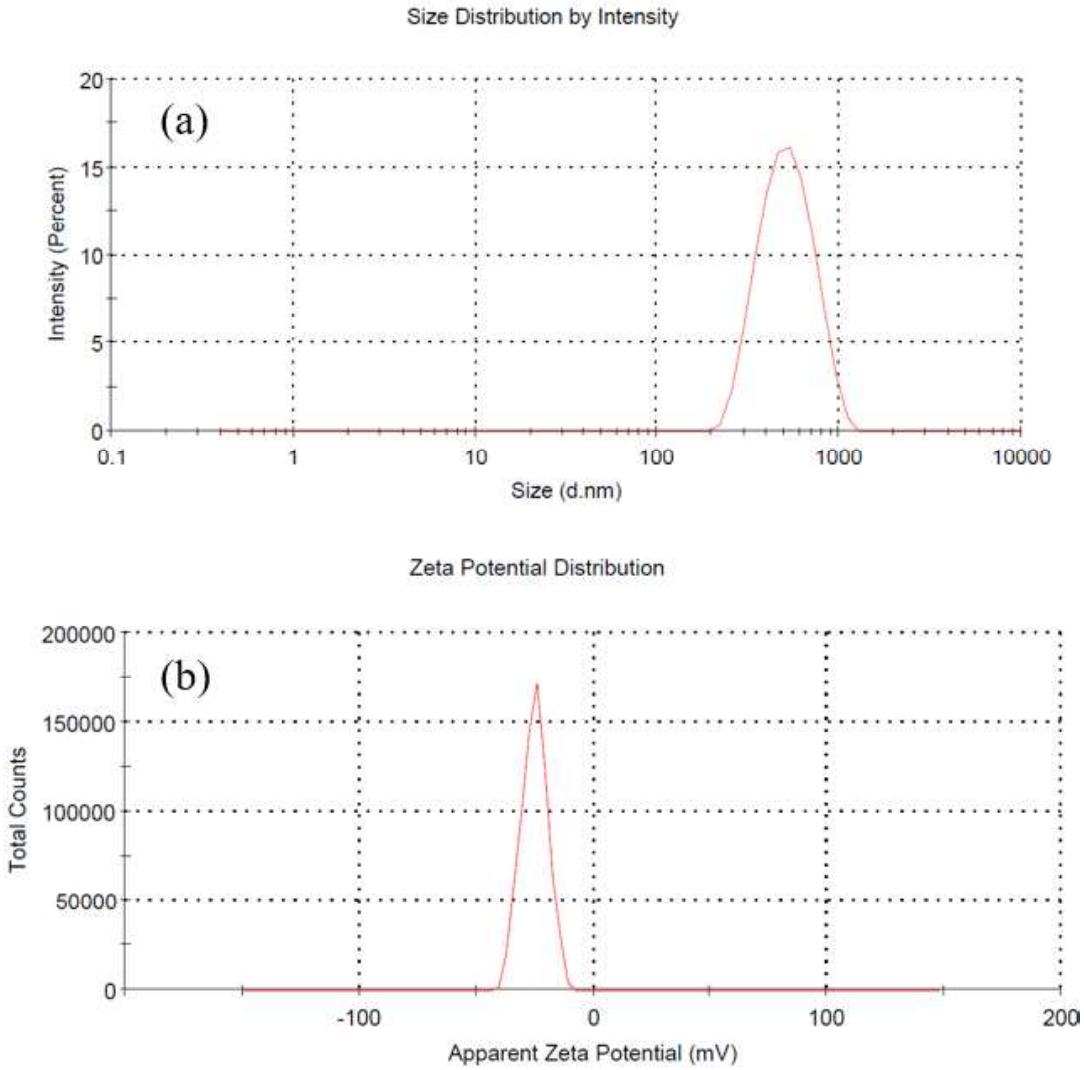

Figure 4.3. (a) Particle size distribution (Standard deviation: 176.5 nm, Intercept: 0.801, % Intensity: 100) and (b) Zeta Potential Distribution (Standard deviation 5.61 mV, Area %: 100) of Anatase Titanium (IV) oxide (TiO_2)

4.3.2 AB 113 photocatalytic oxidation

Photocatalytic oxidation of AB 113 reasonably enhanced the biodegradability index (i.e., BOD/COD) of wastewater. The biodegradability index of wastewater was increased from 0.21 ± 0.0062 to 0.395 ± 0.0058 after 90 min of UV irradiation (**Figure 4.4**). COD and TOC concentrations gradually declined during photocatalytic oxidation by generating highly reactive hydroxyl radicals. After 90 min, the COD was reduced from 1256 ± 22.8 mg/L to 628

± 11.4 mg/L, whereas TOC was reduced from 678.8 ± 13.9 mg/L to 126.8 ± 6.34 mg/L, respectively. The pre-oxidation treatment, however, to some extent mineralized the dye, which supports the biological degradation. A similar study was carried out for the treatment of gardenia-yellow-manufacturing wastewater through a combination of photocatalytic oxidation ($K_2S_2O_8$-doped-TiO_2 used as a photocatalyst) and batch bioreactor (He et al., 2020). The BOD_5/COD ratio improved from 0.08 to 0.34, whereas COD (382.4 to 250.3 mg/L) and TOC (158 to 125 mg/L) concentrations were also gradually reduced after 180 min illumination with visible light irradiation. In another study, the photocatalytic pre-oxidation (Anatase TiO_2 used as a photocatalyst) enhanced the biodegradability index (BOD/COD) of Crystal Violet dye with 99% removal efficiency attained after a reaction period of 4 h (Chen et al., 2013). The photocatalytic oxidation of AB 113 not only reasonably enhanced the biodegradability index but also significantly alleviate the extent of dye removal. The preliminary photocatalytic oxidation study was carried out based on the variation of photocatalyst loading, initial solution pH, and AB 113 concentration**.**

The relationship between COD and TOC was indeed expected to be linear, reflecting the conversion of organic carbon compounds into their oxidized forms. The data presented in Figure 4.4 was derived from instrumental measurements, and the observed non-ideal response indeed deviates from the anticipated linear correlation. The deviation from linearity observed in the later stages of irradiation was attributed to the presence of certain non-ideal responses within the system. These non-ideal responses may arise due to various factors such as the formation of intermediate by-products, the influence of reaction kinetics, or the occurrence of other concurrent phenomena during the degradation process. Additionally, non-linear behavior could be exhibited due to the presence of various co-existing compounds or unforeseen reactions during the experimental timeframe.

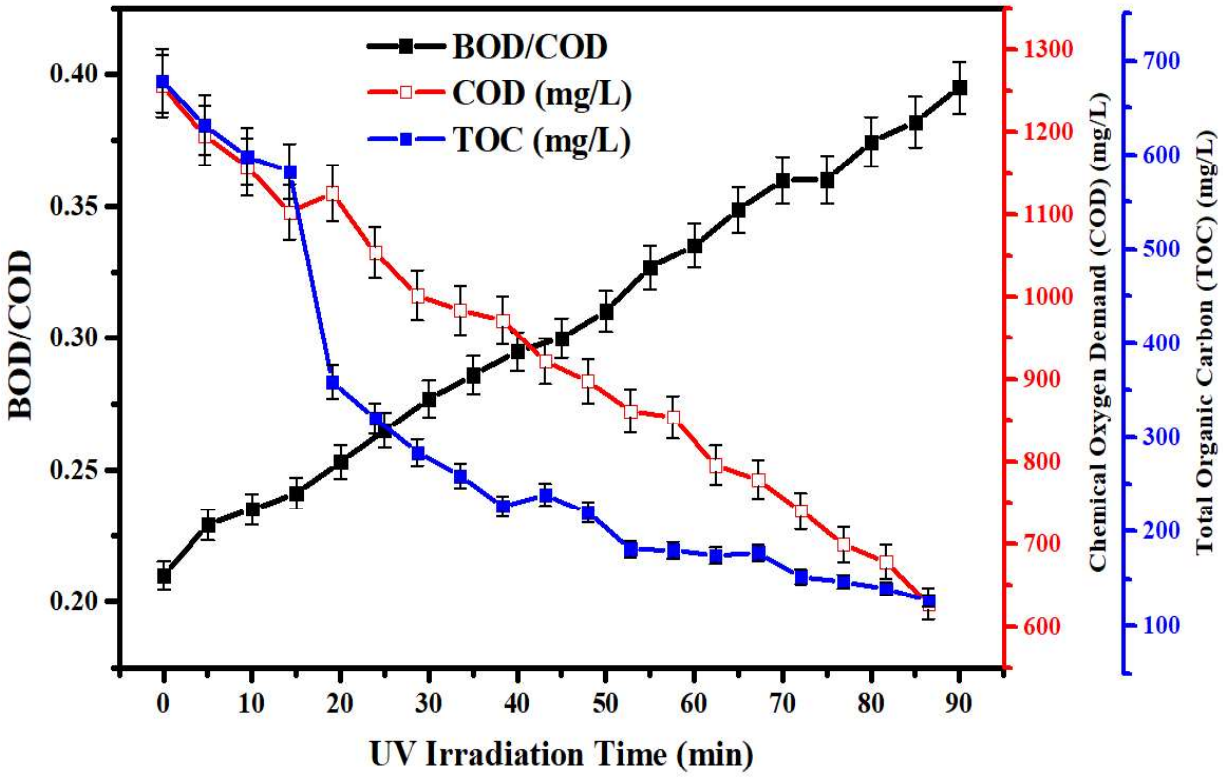

Figure 4.4. Photocatalytic oxidation of AB 113: BOD/COD ratio i.e., Biodegradability index steadily rises during oxidation; Chemical Oxygen Demand (COD); and Total Organic Carbon (TOC) reduction during photocatalytic oxidation (Error bars depict the standard deviation)

4.3.2.1 Effects of TiO_2 loading

TiO_2, as a photocatalyst, accelerates the oxidation of organic compounds (Kanakaraju et al., 2018). The generated reactive oxidation species (ROS) (i.e., OH•) merely attack the dye molecule, subsequently, oxidation occurs. As the catalyst loading increased, the active surface area for adsorption of dye molecules increased which facilitated the mineralization of dye molecules. The amount of TiO_2 was successively varied; meanwhile, the intensity of UV irradiation remained constant (2.0×10^{-3} E s^{-1}) and examined the AB 113 removal efficiency. As the catalyst loading increased from 0.5 to 1.5 g/L, the dye removal improved from 82.5 ± 0.21% to 86.42 ± 0.33% (**Figure 4.5a**). That could be due to more active sites available for the adsorption of dye molecules and enhanced degradation efficiency. The possible reason that

could be attributed to the above findings was the formation of nitrobenzene, aniline, and their derived compounds (Bansal et al., 2010). These compounds were stable and did not further undergo oxidation (Jafari et al., 2012; Li et al., 2022). Additionally, the Mesomeric effect (-M effect) was also liable for the more stability of $–NO_2$ containing functional groups. Due to the –M effect, electron density retarded as the functional group ($–NO_2$) withdraw electrons due to the delocalization, and electron density decreased. The solution had become more opaque as the TiO_2 loading increased. As a consequence, the dye removal efficiency declined and achieved a 72.65 ± 0.19% removal efficiency corresponding to the TiO_2 concentration of 3.5 g/L. The highly opaque solution attenuated the UV irradiation intensity, and the aggregation of TiO_2 particles resulted in the reduction of active sites. The obtained results were in good agreement with the studies carried out by (Mortazavian et al., 2019). They reported a threshold catalyst dose for AB 113 photocatalytic degradation was 2 g/L, beyond that amount degradation declined. An optimum amount of TiO_2 was 1.5 g/L which gave a maximum extent of dye removal and also made the solution less opaque and facilitated the generation of OH•.

4.3.2.2 Effects of pH

Changing the pH of the solution can influence the photocatalyst's and contaminant's adsorption mechanism and surface charge functionalities. As a result, the effect of pH on the degradation of the AB113 dye was investigated. AB 113 removal efficiency declined from 87.56 ± 2.38% to 34.68 ± 1.73% as the pH varied from 3 to 11 (**Figure 4.5b**). The remarkable declination in removal efficiency at an alkaline pH was due to the presence of large numbers of hydroxyl ions (OH^-), which prevented anionic dye molecules from adhering to the photocatalyst. The point of zero charge (PZC) of anatase TiO_2 was 6.1 (Zeng, 2013). The particle surface charge remained positive below 6.1 and negative above 6.1. AB113 has two sulfonates ($-SO_3^-$) groups, is negatively charged, and is protonated at pH below its acid dissociation constant (pKa) of 0.5

(Al-Musawi et al., 2022). Therefore, strong adsorption between dye molecules and TiO_2 particles occurred at an acidic pH. Alkaline circumstances, on the other hand, allow for the development of repulsive electrostatic contacts between anionic dyes and the negative surface of photocatalysts. Another similar analysis also reported that AB 113 had achieved its maximum removal efficiency at pH 3 and removal efficiency progressively decreased as pH increased to 11 (Al-Musawi et al., 2022). The acidic environment was responsible for a more electrostatic attraction between AB 113 and anatase TiO_2, therefore a maximum amount of dye was adsorbed on the surface of TiO_2 and oxidized.

4.3.2.3 Effects of AB 113 Concentration

AB 113 removal efficiency decreased from 84.36 ± 2.2% to 27.8 ± 1.39% as the concentration was successively increased from 50 mg/L to 500 mg/L at an irradiation duration of 90 minutes (**Figure 4.5c**). Although the photocatalyst dose and UV intensity were all constant, a definite number of the e^-/h^+ couple was generated for dye decomposition. During photocatalysts, high concentrations of the AB113 dye reduced the frequency of photon adsorption on the surface of the catalyst. This phenomenon had led to a significant reduction in the generation of reactive hydroxyl species (OH•) and, as a corollary, a lowering in photocatalytic degradation. Previous researchers had also reported that the performance of the photocatalytic process was reduced with the increasing concentration of pollutants (Balarak and Mostafapour, 2019; Mortazavian et al., 2019). A high amount of AB 113 (500 mg/L) attenuated the irradiation intensity and reduced the oxidation rate, therefore dye removal was decreased to 27.8 ± 1.39%.

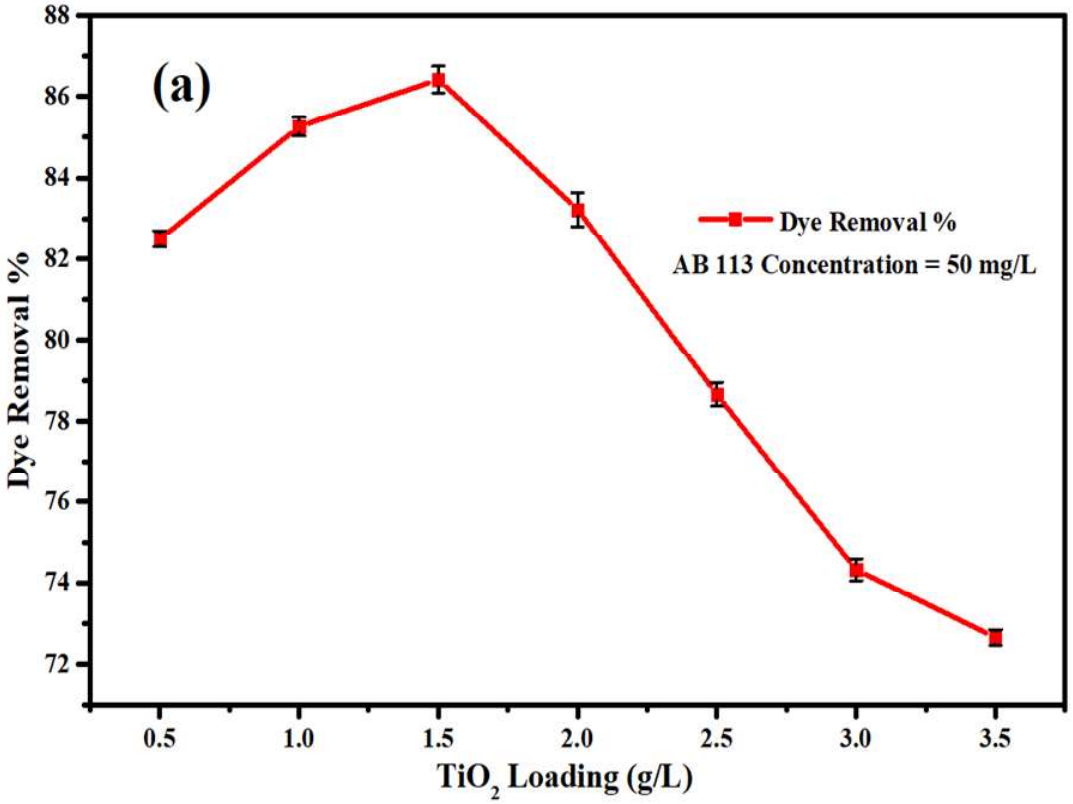
(a)
Dye Removal %
AB 113 Concentration = 50 mg/L
Dye Removal %
TiO2 Loading (g/L)
88
86
84
82
80
78
76
74
72
0.5
1.0
1.5
2.0
2.5
3.0
3.5

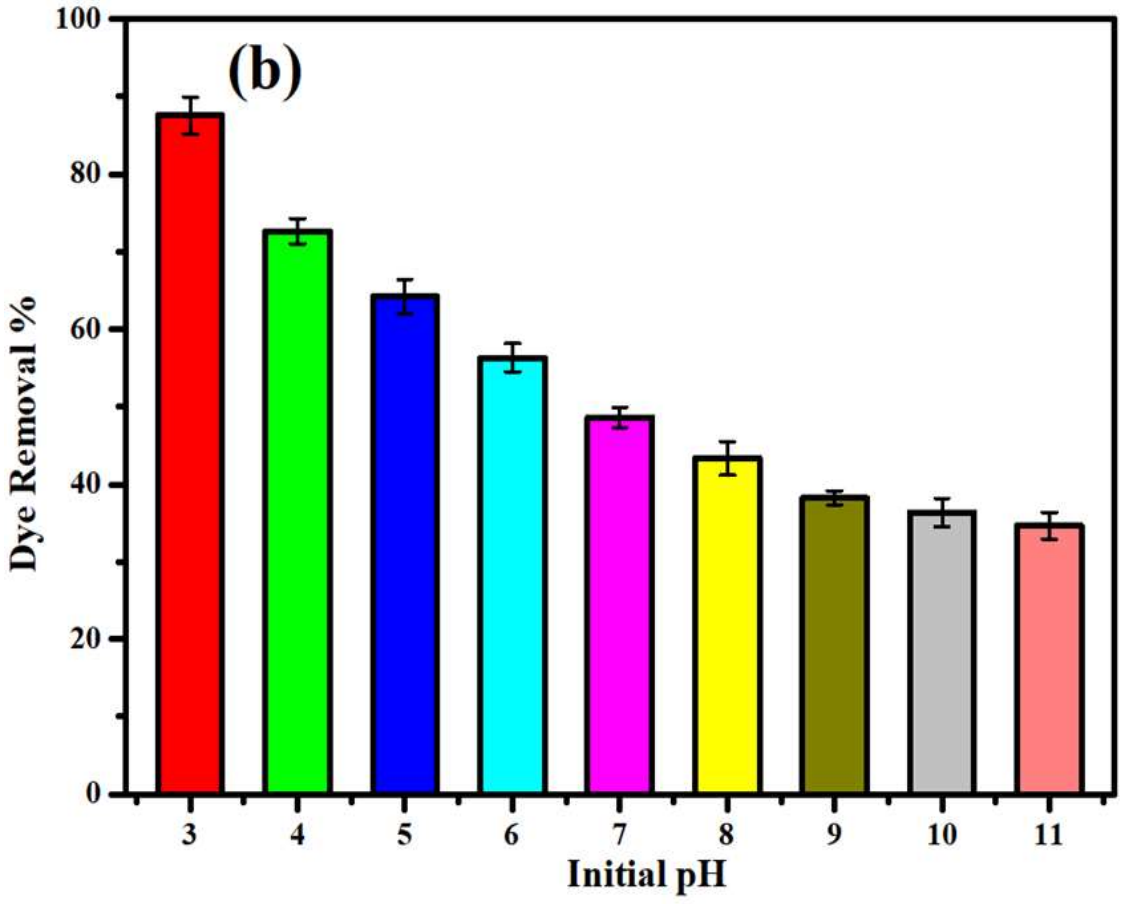
(b)
Dye Removal %
Initial pH
100
80
60
40
20
0
3
4
5
6
7
8
9
10
11

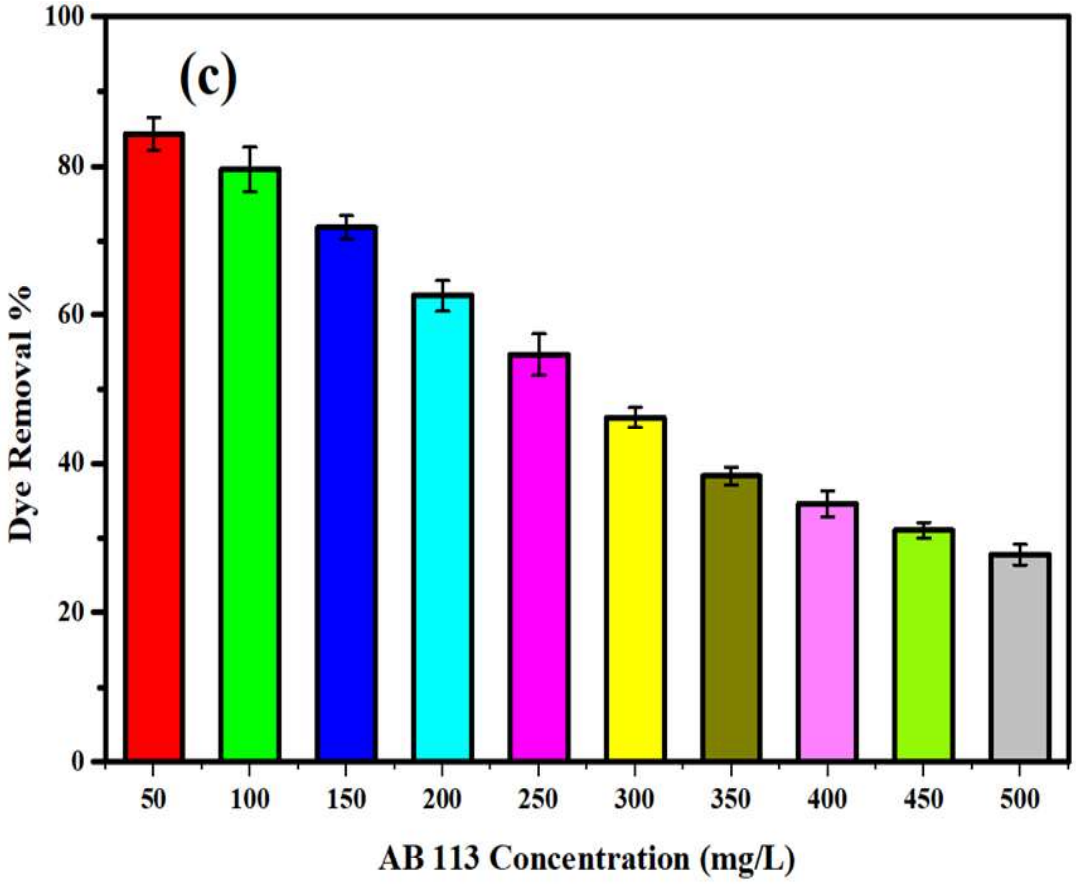

Figure 4.5. Photocatalytic oxidation of AB 113 and its removal efficiency. (a) Effects of TiO_2 loading; (b) Effect of initial pH; (c) Effect of Dye concentration

4.3.3 AB 113 Biodegradation study

It is reported that wastewater shows poor biodegradability when it has a low biodegradability index (< 0.2) (Thorat and Sonwani, 2022). Therefore, wastewater was first partially oxidized in the photocatalytic reactor (90 minutes) to enhance the biodegradability index and then fed to the FBR under different retention times. To assess the FBR applicability for the efficacious performance, a stand-alone AB 113 (300 mg/L) biodegradation analysis was carried out. The maximum AB 113 dye removal efficiency of 64 ± 2.1% was obtained when it was treated in FBR only. This could be due to the low biodegradability index of AB 113 (BOD/COD = 0.21 ± 0.0062). A comparative analysis of AB 113 removal efficiency was carried out in a standalone FBR system and an integrated PC-FBR system. Meanwhile, the integrated reactor

system achieved a maximum of 92 ± 2.6% dye removal efficiency at the retention time of 120 hours (**Figure 4.6**).

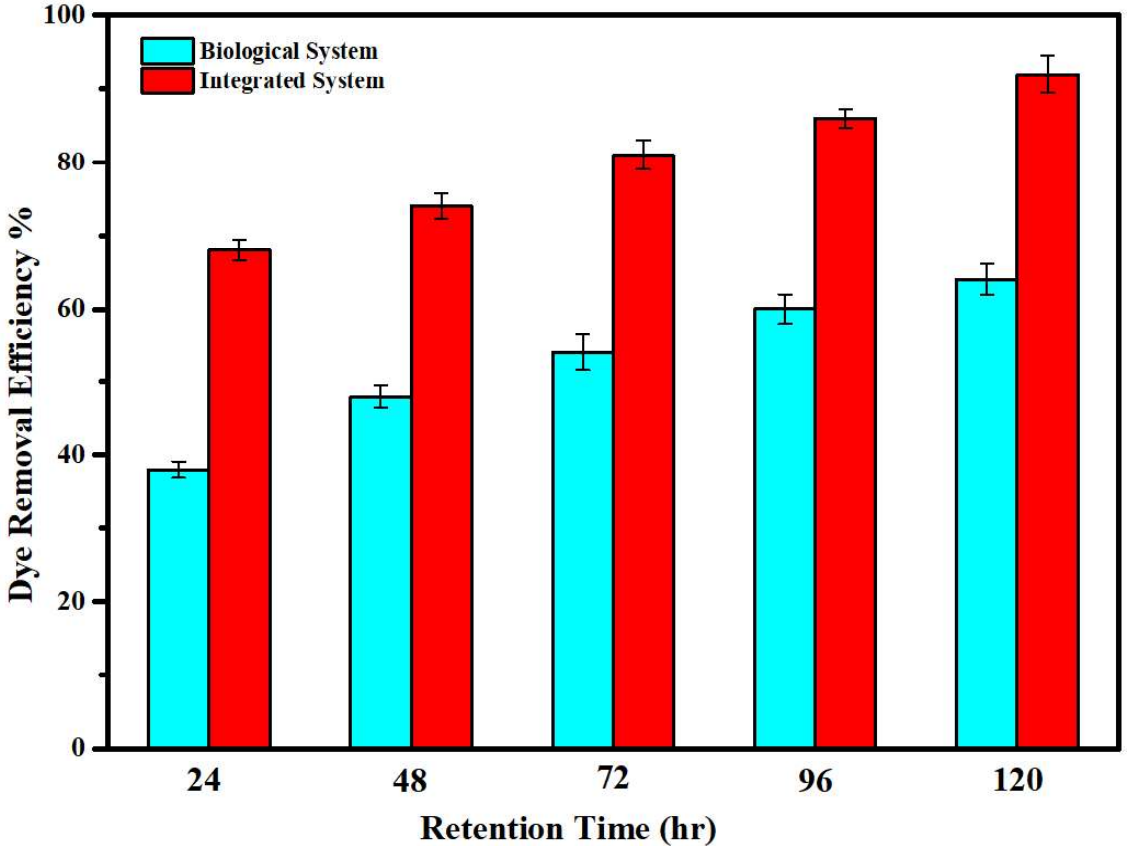

Figure 4.6. A comparative study of AB 113 dye removal using integrated and purely biological methods (AB 113 concentration: 300 mg/L; pH: 7± 0.5; Temperature: 30 ± 5 ◦C) (Error bars depict the standard deviation)

Further, the performance of the integrated system declined as the dye concentration was further increased beyond 300 mg/L. UV-Visible absorbance spectral analysis (at λ_{max} of 550 nm) revealed that the absorbance of AB 113 gradually declined during various intermediate phases of treatment (**Figure 4.7**).

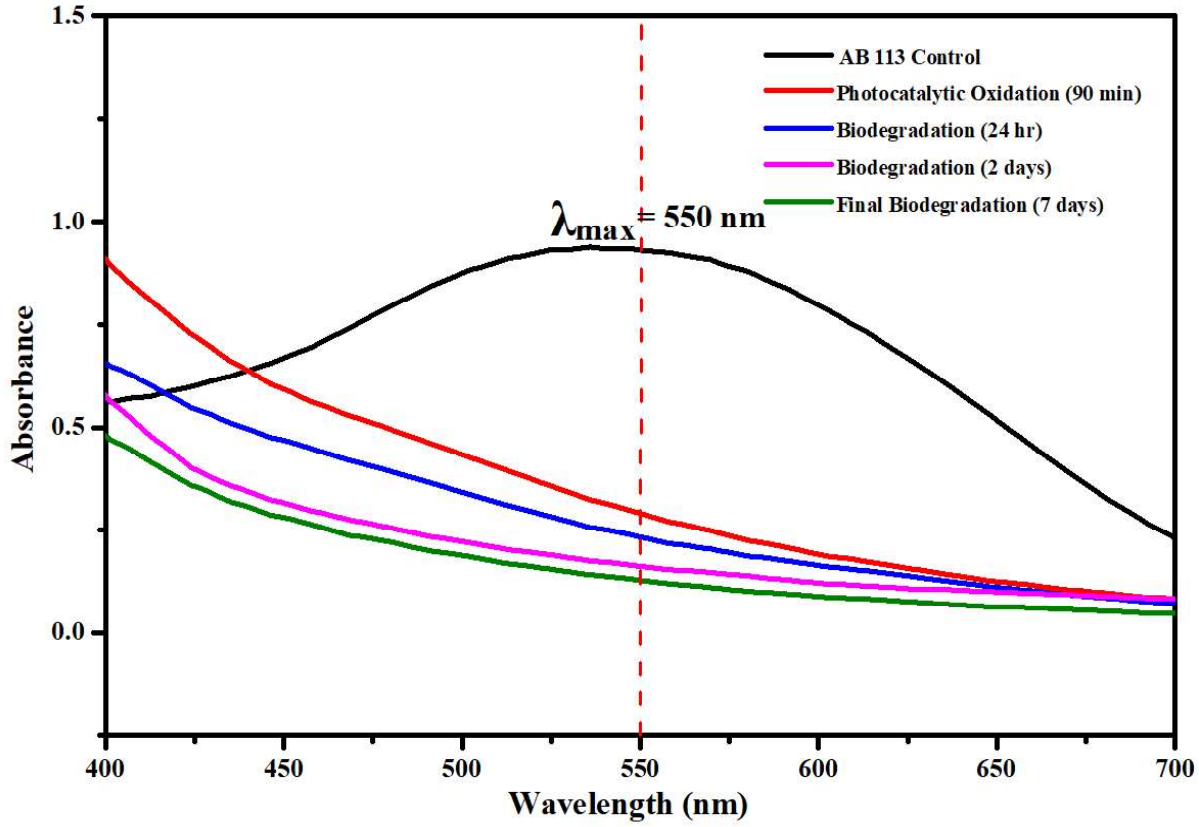

Figure 4.7. Typical UV- Visible spectra of AB 113 during various phases of treatment

4.3.4 Effect of shock loads on the performance of biological systems

The continuous and shock-loading removal efficiency of AB 113 has required for a typical bioreactor system to be convenient at an industrial scale for the treatment of textile effluents. The tendency of the bioreactor to tolerate shock loads and the potential to restore effectively were the two main criteria included in this bioprocess to evaluate bioreactor effectiveness. The effects of operational parameters namely AB 113 concentration, retention time, and AB 113 shock loads on the AB 113 removal efficiency within a typical FBR system were assessed. Despite the flow rates, the results revealed that the control bioreactor (without bacteria immobilized) showed very negligible dye removal efficiency. In FBR, as the flow rate and dye shock loading continued to increase, the removal efficiency declined (**Figure 4.8**).

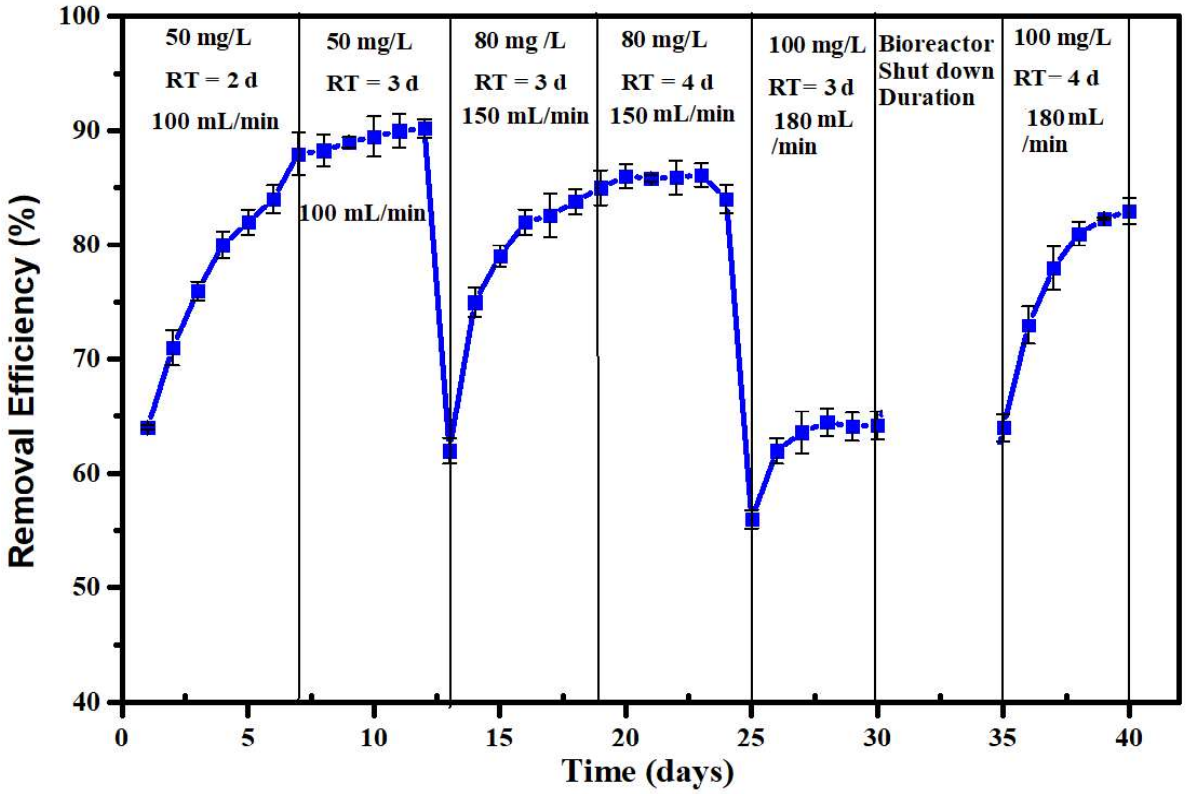

Figure 4.8. Influence on removal efficiency of AB 113 at various shock loading within a typical biological reactor system (AB 113 concentration: 100 mg/L; Shock loading: 50, 80, and 100 mg/L; Bacterial cells: 5× 10^6 CFU/mL; Flow rates: 100, 150, and 180 mL/min; pH: 7 ± 0.5; Temperature: 30 ± 5 ◦C; RT stands for retention time of AB 113 dye shock loads) (Error bars depict the standard deviation of triplicate study)

The FBR exhibited a maximum of 90.2 ± 0.8% removal efficiency after an exposure of 50 mg/L of shock loading having a flow rate of 100 mL/min. The bioreactor attained 86.1 ± 1.05% and 83 ± 1.15% of removal efficiency after exposure to shock loading of 80 mg/L and 100 mg/L having a corresponding flow rate of 150 mL/min and 180 mL/min, respectively. Also, shock loading or possible intermediate toxicity had a short-lived influence. Therefore, only two to three-day recovery periods were necessary to achieve favorable removal efficiency after shutting down the biodegradation process. Continuous biofilm reactors performed less well

against shock loads as a direct consequence of stratification and non-uniform biomass concentration (Oberoi and Philip, 2017). A similar kind of study had reported for Ethyl violet containing wastewater with Raschig rings as a packing material within a packed bed bioreactor (PBR) to assess the effect of shock loading (Chen et al., 2014). The suppression of shock loading and the recovered dye removal efficiency of 83 ± 1.15% indicated that FBR has suitability to treat complex wastewater.

4.3.5 Kinetics Study

4.3.5.1 Photocatalytic oxidation kinetic study

For the photocatalytic oxidation of AB 113, Langmuir reaction rate constant (k_c) and adsorption equilibrium constant (K_C) were obtained from the slope and intercept of the plot between $\frac{1}{k_{approx}}$ and initial dye concentration (C_o). The dye decolorization was allowed to obey the kinetic model up to 100 mg/L of dye concentration. It is reported that more UV light blocking by dye itself was indeed the main reason for the not applicability of the model at higher concentration levels. A linear relationship between $\frac{1}{\mathrm{k_{approx}}}$ and C_o has presented a slope $\left(\frac{1}{k_c}\right)$ of 0.27767 and an intercept $\left(\frac{1}{k_c K_c}\right)$ of 3.938 with a corresponding coefficient of regression R^2 = 0.9842 (**Figure 4.9**). The Langmuir reaction rate constant (k_c) and the combined adsorption equilibrium constant for the dye and its intermediates (K_c) on the irradiated TiO_2 surface were found to be 3.6014 min^{-1} and 0.0705 L/mg, respectively.

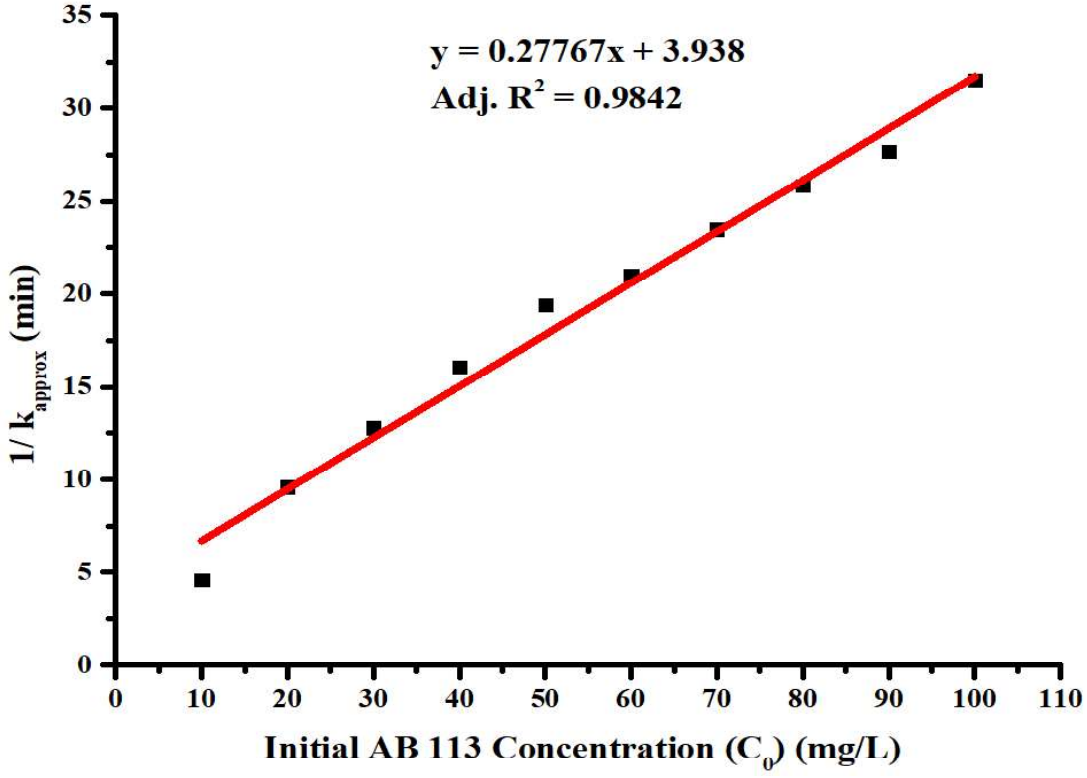

Figure 4.9. The modified Langmuir– Hinshelwood kinetic model for the photocatalytic oxidation of AB 113 on TiO_2

4.3.5.2 Biodegradation kinetic study

To determine the kinetic parameters for non-inhibition and substrate inhibition, Monod and Andrew-Haldane models were employed. It was found that the specific growth rate (μ) of bacteria was increased with concentration up to 125 mg/L; after this stage, the value of μ continuously declined. The maximum specific growth rate (μ_{max}) and half-saturation constant (K_s) values were obtained to be 0.123 day^{-1} and 44.5 mg/L, respectively (**Figure 4.10**). The value of $\frac{\mu max}{K_s}$ has been recognized as an essential quantitative index to demonstrate the degrading potential of microorganisms (Geed et al., 2017). According to the Andrew-Haldane model, the kinetic parameters, i.e., maximum specific growth rate (μ_{max}), half-saturation constant (K_s), and substrate inhibition constant (K_i) under substrate inhibition were determined to be 0.176 day^{-1}, 48.5 mg/L, and 130 mg/L, respectively (**Figure 4.10**).

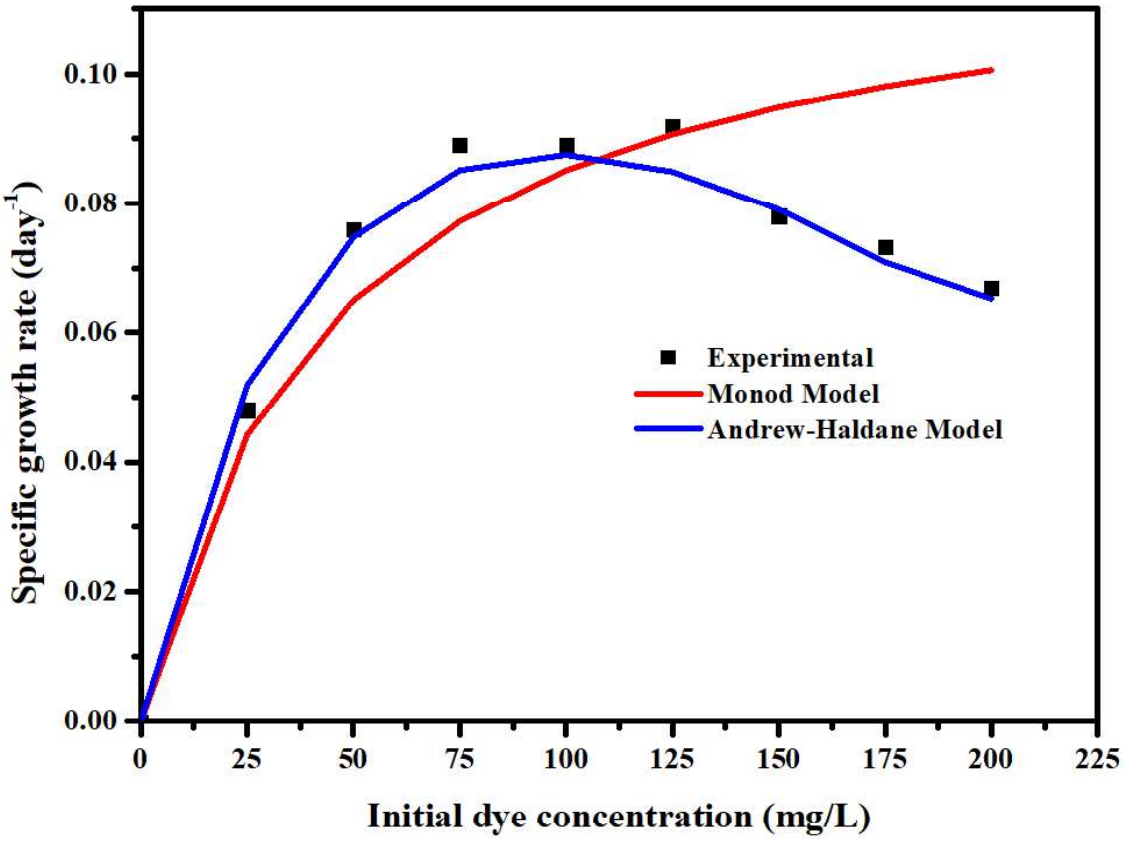

Figure 4.10. Experimental and model-prediction graphs of Growth Kinetics fitted by Monod model, and Andrew-Haldane model for the biodegradation of Acid Blue 113 dye

The $\frac{\mu_{max}}{K_s}$ values were obtained as 0.002764 and 0.003629 L/(mg. day) for Monod and Andrew Haldane models, respectively. The influence of Acid Orange 7 dye concentration (range varying from 50 to 200 mg/L) on the bacterial growth rate was investigated using the Andrew-Haldane model (Swain et al., 2021). They found that the corresponding kinetic constants; μ_{max}, K_s, and K_i were 0.061 day^{-1}, 37.47 mg/L, and 631.97 mg/L, respectively. The kinetics of Congo Red (50-300 mg/L) biodegradation in a packed bed bioreactor were fitted with the Andrew-Haldane model (Maurya et al., 2022). They reported that the values of μ_{max}, K_s, and K_i were obtained to be 0.295 h^{-1}, 50.32 mg/L, and 10.54 mg/L, respectively.

4.3.6 FTIR analysis of AB 113 degraded products

The FTIR spectral analysis of AB 113 showed the major peaks at 3451.2 cm^{-1} (secondary amine, medium N-H stretch), 1632.4 cm^{-1} (azo bond, N=N), 1135 cm^{-1} (Aromatic amine, variable C-N stretch), 736.7 cm^{-1} (Aromatic ring, benzene derivative C-H strong bend), and 610.7 cm^{-1} (Alkene, strong and broad C-H bend) (Zayani et al., 2008) (**Figure 4.11a**). TiO_2-assisted photo-catalytically oxidized samples exhibited the major peaks at 3411.4 cm^{-1} (Phenol, strong and broad O-H stretch) (Yilmaz et al., 2022), 2897.2 cm^{-1} (Carboxylic acid, variable and broad O-H stretch), 2604.9 cm^{-1} (aldehyde, medium C-H stretch), 1697.2 cm^{-1} (benzene derivative amide or acid, C=O stretch), 1393.13 cm^{-1} (Nitro compound, strong asymmetric N-O stretch), 1168.9, and 1054.8 cm^{-1} (aliphatic amines, variable C-N stretch), 820.9 cm^{-1} (primary and secondary amine, strong and broad N-H wag) (**Figure 4.11b**). The di-azo linkage of AB 113 disappeared after the photocatalytic oxidation. The obtained oxidation products were Nitro compounds ($R\text{-}NO_2$), Phenol, benzene derivative Carboxylic acid, Aldehyde, and Amide, respectively. This was obtained due to the oxidation of N=N, N-H, C-N, and C-H bonds of AB 113.

The biodegraded products exhibited the major peaks at 3311.8 cm^{-1} (amide N-H, alkyne C-H, or O-H bond of alcohol), 2111.9 cm^{-1} (Nitrile, variable C≡N stretch), 1609.7 cm^{-1} (either alkene, medium C=C stretch or primary amine, medium N-H bend (Joshi et al., 2022), and 1400 cm^{-1} (Alkane, medium C-H bend, rock) (**Figure 4.11c**). The above findings were obtained due to the bacterial reduction of aromatic amide, carboxylic acid, and nitro compounds. The presence of alkene and alkane significantly suggested that the most of aromatic compound's rings opening occurred. The TiO_2-assisted photocatalytic oxidation of AB 113 degraded the di-azo linkage and oxidized into the Nitrobenzene-derived compounds, which had not further undergone oxidation. The biodegradation facilitated the degradation of nitrobenzene-derived compounds into further simpler compounds. A comparative spectral analysis suggested that

AB 113 dye initially oxidized into a nitro, amide, and carboxylic acid and the biological reduction further formed the simple reduced aliphatic compounds. The above findings were attributed to the fact that complete mineralization of biorecalcitrant AB 113 dye occurred.

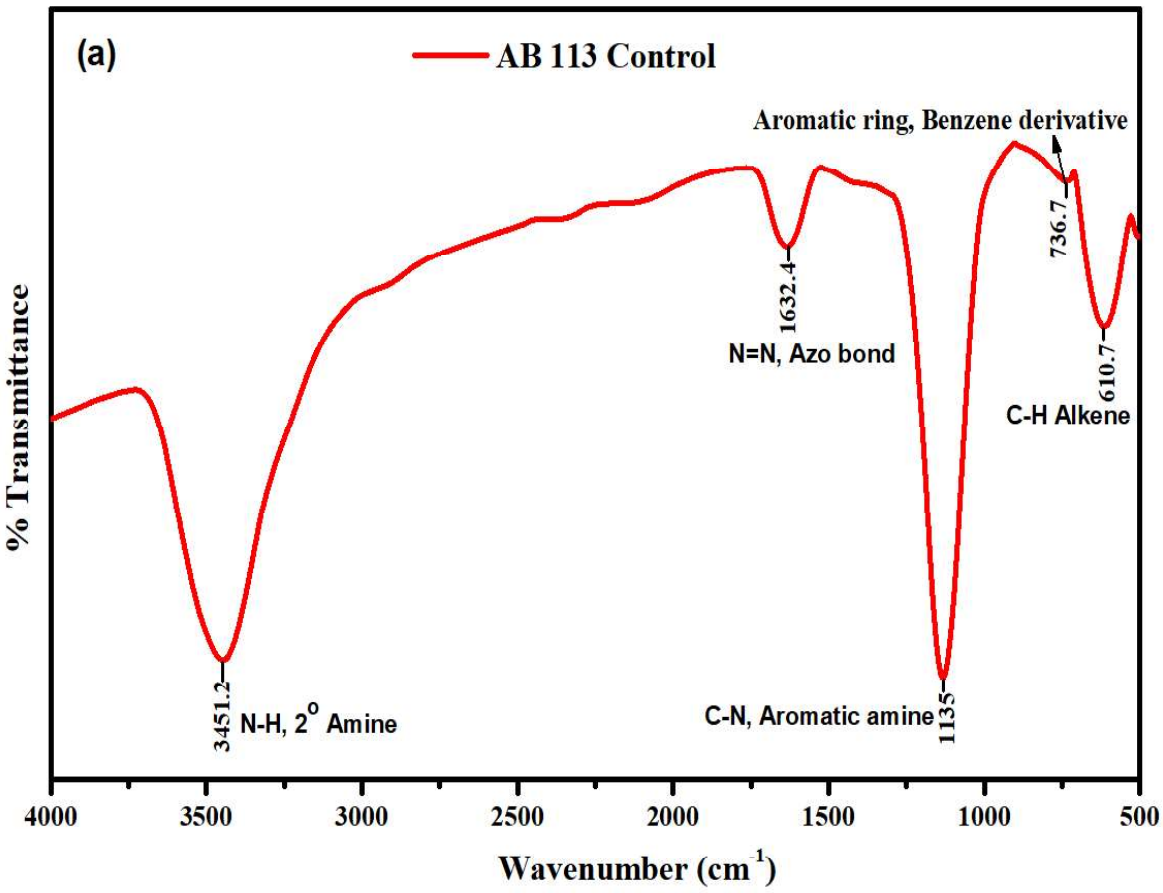

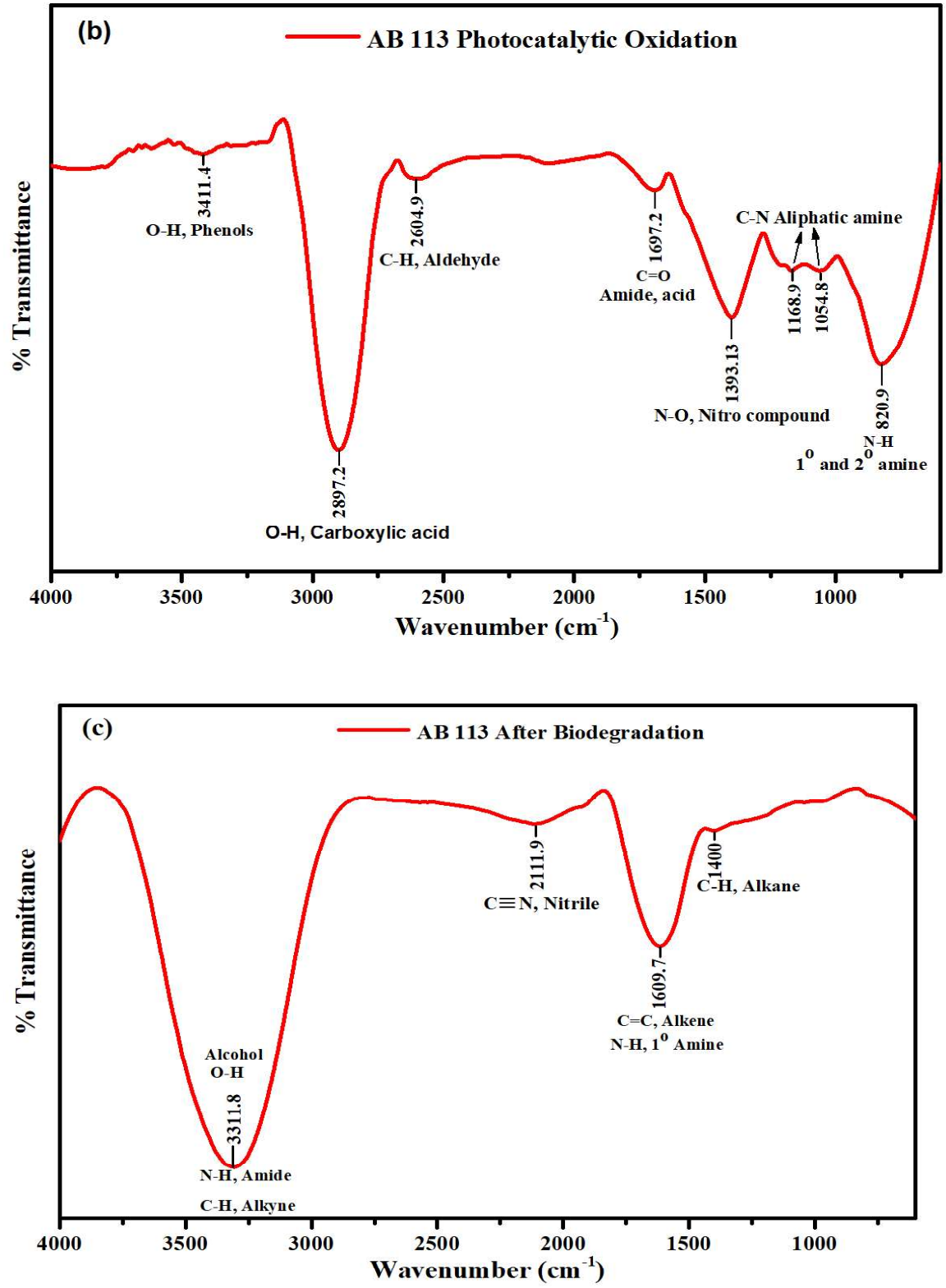

Figure 4.11. FTIR Spectra (a) Acid Blue 113; (b) AB 113 photocatalytic oxidized products; (c) FBR final biodegraded products

4.3.7 Toxicity assessment using bacterial toxicity

The bacterial toxicity assessment of untreated AB 113, photocatalytic oxidized, and biodegraded samples were analyzed based on the bioluminescence intensity of the *Pseudomonas fluorescens.* To determine the acute and chronic toxicity, the bioluminescence intensity of *P. fluorescens* in various water samples was assessed after 30 min and 24 h, respectively. The bioluminescence intensity of *P. fluorescens* (at 504 nm) after acute exposure to AB 113 receded to 11.33×10^5 counts per second to the control (distilled water) sample having an intensity of 32.24×10^5 counts per second (**Figure 4.12a**). The intensity peak of photocatalytic oxidized (10.91×10^5 counts per second) was nearly close to that of the AB 113 sample, whereas the intensity peak of biodegraded (23.63×10^5 counts per second) was reasonably higher compared with AB 113. The toxicity of photocatalytic oxidized products was close to the AB 113, the subsequent biodegradation diminished the acute toxicity level as the intensity peak surged. The photocatalytic oxidized products were further mineralized through biodegradation. The acute toxicity level of biodegraded products was significantly reduced. Even after experiencing a longer exposure of 24 h, the biodegradable and photocatalytic oxidized samples further improved the bioluminescence intensities (**Figure 4.12b**).

The percentage of bioluminescence inhibition (BI), an indication of bacterial mortality of *P. fluorescens* during acute and long-term exposure to the untreated and treated dyeing-water samples was calculated using Eq. 4.8 (**Figure 4.12c**). The untreated AB 113 sample exhibited 64.84 ± 3.2% and 68.76 ± 3.4% BI of *P. fluorescens* during acute and chronic toxicities, respectively. After the photocatalytic oxidation of AB 113 in the photoreactor, the photocatalytic oxidized products showed a BI of 66.14 ± 3.3%, which was somewhat higher than AB 113. A possible reason behind this could be the formation of more toxic intermediate

oxidized products. Furthermore, the chronic exposure to photocatalytic oxidized marked 50.38 ± 2.5% BI whereas the biodegraded sample exhibited 42.79 ± 2.1% BI.

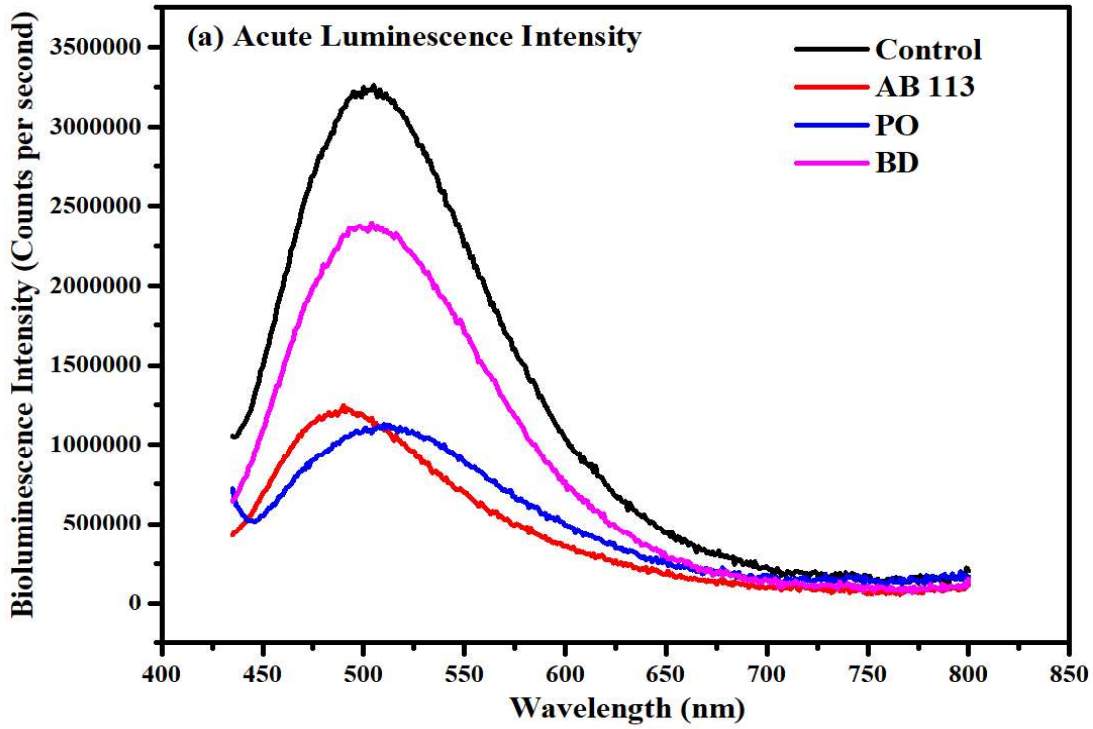

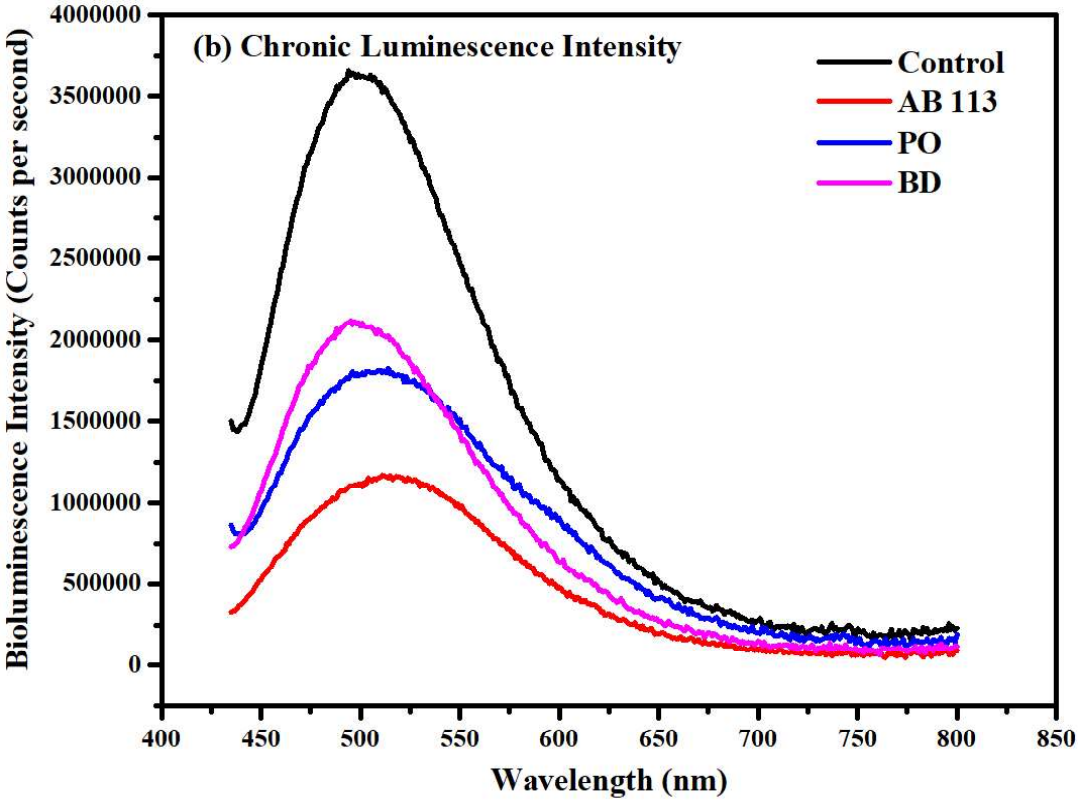

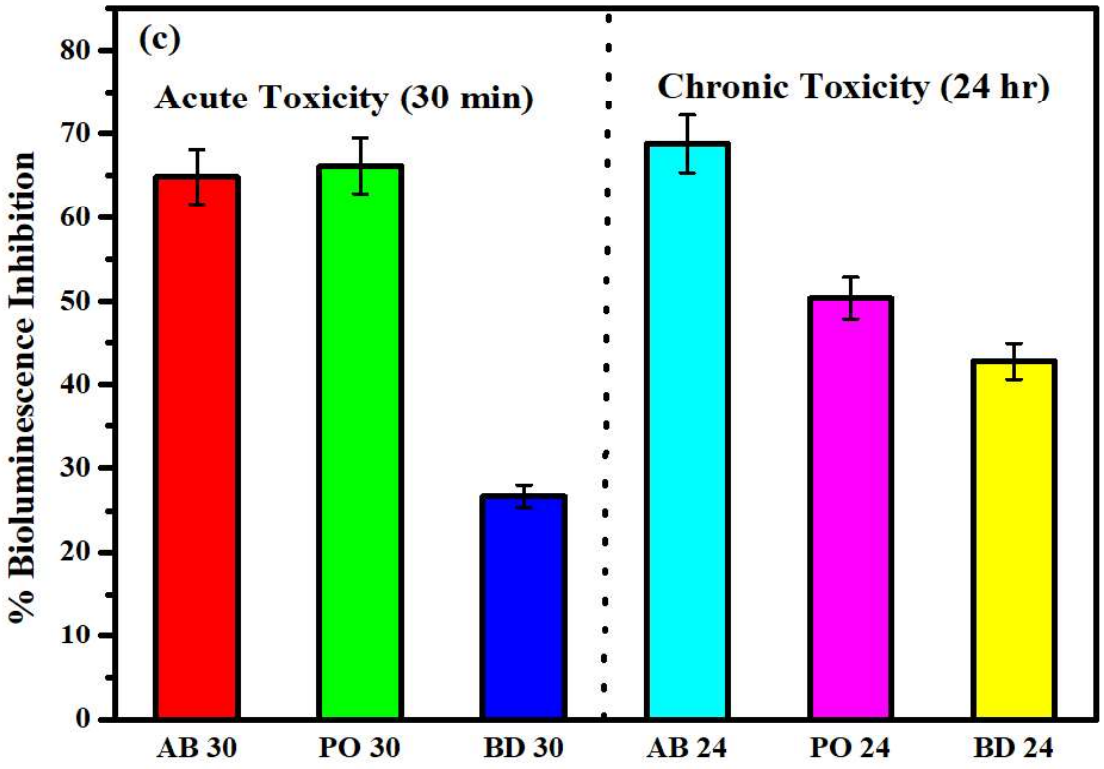

Figure 4.12. (a) Acute and (b) Chronic bioluminescence intensity of Acid Blue 113 (AB 113), Photocatalytically oxidized, Biodegraded products, and Distilled water (Control) samples; (c) A typical Bioluminescence inhibition plot of *Pseudomonas fluorescens* during acute (30 min) and chronic (24 hr) AB 113, photocatalytic oxidized, and biodegraded samples with reference to the control (distilled water). All the data are represented as the mean % BI ± standard deviation of the triplicate study

4.4 Conclusions

The present study is elucidated to evaluate the efficacy of an integrated system (i.e., PC-FBR) for the effective mineralization of AB 113. Initially, the photocatalytic reactor enhances the biodegradability index of wastewater from 0.21 ± 0.0062 to 0.395 ± 0.0058. After that, the wastewater was subjected to a fixed bed bioreactor for further mineralization. An integrated system achieved a maximum of 92 ± 2.6% dye removal efficiency. The degradation kinetics were evaluated by Monod (μ_{max} = 0.123 day^{-1}, K_s = 44.5 mg/L), Andrews-Haldane (μ_{max} = 0.176

day^{-1}, K_s = 48.5 mg/L, K_i = 130 mg/L), and Langmuir– Hinshelwood models (k_c = 3.6014 min^{-1}, K_c = 0.0705 L/mg). Based on the Andrews-Haldane model, the specific growth rate (μ) was increased with concentration up to 125 mg/L, and beyond that, the value of μ continuously decreased. Further, the bacterial toxicity assessment indicated supported that the integrated system was more efficient for the degradation as well as the detoxification of complex AB 113. The integrated system can further be extended to treat a wide range of recalcitrant pollutants.